bioRxiv preprint doi: https://doi.org/10.1101/437236; this version posted October 8, 2018. The copyright holder for this preprint (which was not certified by peer review) is the author/funder, who has granted bioRxiv a license to display the preprint in perpetuity. It is made available under aCC-BY-NC-ND 4.0 International license.

Cytoskeletal tension actively sustains the T cell immunological synapse

Sudha Kumari[1,2]*, Michael Mak[5,†], Yehchuin Poh[1,3], Mira Tohme[6], Nicki Watson[7], Mariane Melo[1,2], Erin Janssen[6], Michael Dustin[8], Roger Kamm[5], Raif Geha[6] and Darrell J. Irvine[1,2,3,4]*#.

1- Koch Institute of Integrative Research, MIT, Cambridge, MA

2- Ragon Institute of Harvard, MIT and MGH, Cambridge, MA 3- Department of Biological engineering, MIT, Cambridge, MA 4- Howard Hughes Medical Institute, Chevy Chase, MD

5- Department of Mechanical Engineering, MIT, Cambridge, MA.

6- Division of Immunology, Boston Children's Hospital, Harvard Medical School, Boston, MA.

7- Whitehead Institute of Biomedical Research, Cambridge, MA.

8- Kennedy Institute of Rheumatology, University of Oxford, Oxford, UK.

† Current address: Department of Biomedical Engineering, Yale University, New Haven, CT.

* Correspondence to kumars04@mit.edu; djirvine@mit.edu.

Lead contact

Keywords: immunological synapse, stop signal, actin cytoskeleton, synapse mechanics, T cell migration

bioRxiv preprint doi: https://doi.org/10.1101/437236; this version posted October 8, 2018. The copyright holder for this preprint (which was not certified by peer review) is the author/funder, who has granted bioRxiv a license to display the preprint in perpetuity. It is made available under aCC-BY-NC-ND 4.0 International license.

Abstract

Immunological synapses formed between T cells and cognate antigen presenting cells (APCs) mediate exchange of biochemical information between T cells and APCs, and the duration of such synapses is a critical determinant of T cell activation and effector functions. While the process of synapse formation has been well-characterized, the cellular processes that regulate synaptic lifetime remain unknown. Here we identify an antigen-triggered cytoskeletal mechanism that actively promotes T cell synapse stability by generating mechanical tension in the plane of the synapse. Cytoskeletal tension is generated by focal nucleation of actin via Wiskott -Aldrich syndrome Protein (WASP) and contraction of the resultant actin filaments by myosin II. Once T cells are activated, WASP is degraded, leading to cytoskeletal re-arrangement, tension decay and consequently, synaptic disengagement. The study identifies a mechanical program within T cells that regulates the lifetime of the T cell-APC synapse.

Introduction

During an immune response, T cells form specialized junctions with cognate antigen presenting cells (APCs) termed 'immunological synapses'[1, 2]. Such synapses provide a stable platform where a number of T cell surface receptors including T cell receptors (TCRs), adhesion, and costimulatory receptors are enriched and engaged with counter-ligands on the APC surface[2, 3, 4]. A sustained, stable synapse is a hallmark of T cell activation, both *in vitro* and *in vivo*[3, 5, 6, 7, 8]. It remains poorly defined how T cells – which are otherwise highly motile[9, 10, 11] – sustain their synapses for prolonged durations. This is a crucial gap in our understanding of T cell immunity since synapse lifetime is a critical determinant of T cell activation, effector function, and differentiation[12, 13, 14, 15].

Integrins, the actin cytoskeleton, and calcium signaling are all known to play important roles in the initial formation of an immunological synapse[16, 17, 18, 19, 20], but their roles in the subsequent maintenance and eventual dissolution of the synaptic contact are unclear. For example, integrin activation and actin polymerization are essential processes for T cell adhesion and synapse formation, but these processes could also terminate the synapse by engaging new adhesions and cellular protrusions, respectively, and thus driving T cell migration away from the APC. Furthermore, T cells are inherently highly migratory and have vigorous F-actin dependent lamellar undulations[21, 22] even in the synaptic phase. These lamellar dynamics could promote polarization and lateral movement of the T cell[23], thereby breaking the synapse. F-actin along with the activated integrin lymphocyte function-associated antigen-1 (LFA-1) is organized into a ring-like structure in the early synapse and this ring-like pattern is thought to promote synaptic junctional stability[24, 25, 26]. However, this F-actin/Integrin ring undergoes

bioRxiv preprint doi: https://doi.org/10.1101/437236; this version posted October 8, 2018. The copyright holder for this preprint (which was not certified by peer review) is the author/funder, who has granted bioRxiv a license to display the preprint in perpetuity. It is made available under aCC-BY-NC-ND 4.0 International license.

continuous fluctuations and therefore might also drive synapse breaking[21, 23, 27]. In addition, there exist genetic lesions in actin regulatory proteins such as the Wiskott-Aldrich Syndrome Protein (WASP), where T cells are able to adhere to and form synapses with APCs, but the resultant synapse are highly unstable[21, 28, 29, 30, 31]. Thus, the role of the basic motility apparatus, especially the actin cytoskeleton, in sustaining T cell-APC contacts is complex and warrants further investigation.

Maintenance of the immune synapse is known to be influenced by T cell-intrinsic factors including the strength of TCR signaling[32, 33] and engagement of negative regulatory costimulatory receptors such as CTLA-4 and PD-1[34, 35], however the downstream mechanisms at the level of the cellular migration machinery that enact the transition from an arrested to a motile state are not clear[12, 13, 15, 36]. One of the ways in which the actin cytoskeleton could enforce synapse stability is by regulating mechanical forces at synapse. Polymerization of actin is known to generate forces[37], and organization of the polymerized F-actin network tunes the magnitude these forces[38, 39]. Notably, adhesion forces in T cell-APC conjugates are actin-cytoskeleton-dependent and continue to evolve after initial synapse formation[40, 41, 42, 43], raising the possibility that a specialized F-actin organization and associated forces may regulate maintenance of the synaptic contact.

We hypothesized that an examination of the actin cytoskeleton and associated forces in T cells transitioning from an arrested to a motile state during early activation would provide important clues to the cytoskeletal design principles that T cells employ for maintaining the immune synapse. We examined the cytoskeletal organization at different stages of T cell activation using a combination of super-resolution imaging, genetic and pharmacological perturbations, micromechanical measurements, and computational simulations, using both model APC-mimetic surfaces and physiological APCs. We found that a network of fibers formed between specialized actin microstructures termed actin foci generate intracellular tension in the T cell at the contact interface, and this network actively sustains the synapse after its formation. This process relies on continuous nucleation of actin at TCR microclusters by Wiskott -Aldrich syndrome Protein (WASP), and interaction of freshly polymerized actin filaments with myosin II. Myosin contractile activity generates and maintains high in-plane tension across the synaptic interface. This high-tension actomyosin network eventually breaks as activated T cells downregulate WASP, leading to immediate relaxation of cytoskeletal tension followed by synaptic unraveling and resumption of motility. Taken together, these results uncover a novel antigen-induced biomechanical program that regulates synapse lifetime in primary T cells, and highlight sub-synaptic actin architectures that tune the duration of their interactions with APCs.

bioRxiv preprint doi: https://doi.org/10.1101/437236; this version posted October 8, 2018. The copyright holder for this preprint (which was not certified by peer review) is the author/funder, who has granted bioRxiv a license to display the preprint in perpetuity. It is made available under aCC-BY-NC-ND 4.0 International license.

Results

Synapse maintenance during T cell activation is associated with actin foci but not integrin activation or calcium signaling

The actin cytoskeleton, integrins, and intracellular calcium flux all play important roles in mediating initial T cell motility arrest and formation of a stable synapse with antigen presenting cells. We thus first examined how these factors impact the maintenance of pre-formed synapses. To model synapse formation and eventual disengagement we seeded mouse $CD4^+$ primary naïve T cells (referred to as 'T cells' henceforth) onto an anti-CD3/intercellular adhesion molecule-1 (ICAM-1)-coated coverslip (antigen presenting surface, APS) and allowed synapses to form. We then assessed cellular polarization over time (by recording the cells' morphologic aspect ratio, AR) to detect T cells breaking their synaptic contact, because the contact interface shape is tightly linked to the motility state of the T cell[2, 44, 45, 46] (Fig. 1a, Supp. fig.1a, Supp. fig. 2); synapses are radially symmetric in the stable state, and polarizes to break symmetry and acquire an elongated morphology prior to motility resumption (Supp. Movie 1-2).

Within minutes, T cells seeded on APS spread instantly to form a symmetric contact interface (Supp. fig. 1a). Symmetric synapse persisted for ~10 minutes, followed by a transition period when the cells began polarizing and becoming motile,[2, 44, 45, 46] reflected in elevated AR (Fig. 1b, Movies 1-2). Structured illumination microscopy (SIM) revealed the presence of peripheral actin-rich lamellipodia and punctate actin structures distributed across the synaptic interface (Fig. 1c)– termed 'actin foci'[30]– that are formed at TCR microclusters upon TCR triggering. As T cells began to polarize at later times (20 min), actin foci were reduced while total F-actin levels in the interface remained constant (Fig. 1c-d). Note that the foci quantification methodology we used (employing a Gaussian mask generated by a 1.6x1.6 μm^2 rolling window, as described previously[30]) identified near-complete loss of foci as a ~65% reduction in foci intensity, due to residual signal contributed by the lamellipodial F-actin (Supp. fig. 3). As T cells formed synapses with an APS, the key integrin adaptor protein talin accumulated rapidly at the periphery of the interface; talin levels remained constant at later times as cells began polarizing (Fig. 1d). Activating integrins using $MnCl_2$[47] after a stable synapse was established did not affect subsequent polarization/synapse breaking at 20 min, but inhibiting LFA-1/ICAM interactions using the small molecule inhibitor A286982[48] blocked T cell polarization, indicating that integrin activation is insufficient to sustain synapse symmetry and integrin activation may in fact be required for synapse symmetry breaking (Fig. 1e). Notably, treatment of cells with A286982 was accompanied by a retention of actin foci at 20', supporting a previous report that activated integrins may reduce F-actin accumulation in foci[49]. Under all of the treatment conditions, talin recruitment as well as the total F-actin was unchanged (Fig. 1f left and middle graphs), however, higher actin foci levels were

bioRxiv preprint doi: https://doi.org/10.1101/437236; this version posted October 8, 2018. The copyright holder for this preprint (which was not certified by peer review) is the author/funder, who has granted bioRxiv a license to display the preprint in perpetuity. It is made available under aCC-BY-NC-ND 4.0 International license.

associated with reduced synapse polarization at late times (Fig. 1f, right graph). Elevation of intracellular calcium is a key signal triggering initial arrest and formation of adhesive contacts between T cells and APCs[50]. However, similar to integrin inhibition, blocking calcium signaling in T cells that had formed a synapse using BAPTA[51] induced a retention of actin foci and synapse symmetry at 20' (Supp. fig. 4b). Thus paradoxically, integrins and calcium signaling, which are critical for early T cell arrest and formation of a symmetric synapse following TCR triggering, are also important for synapse symmetry breaking at late times. By contrast, actin foci were clearly enriched in the interface of T cells forming symmetric synapses and reduced or absent as T cells polarized and regained motility under all of these treatment conditions.

T cell polarization is associated with WASP/actin foci downregulation

To directly visualize the dynamics of actin foci as T cells transitioned from the arrested to motile state, we imaged LifeAct GFP-expressing T cells using lattice light sheet microscopy (LLSM) – a technique that exposes cells to lower phototoxicity than traditional microscopy[52], allowing long term imaging of T cell synaptic actin dynamics that was not possible with confocal fluorescence imaging. LLSM imaging revealed that T cells engaged in a stable synapse continuously nucleate and dissipate actin foci across the contact interface, but as the cells polarized to begin migration, pre-existing foci were lost and new foci ceased to form (Fig. 2a; Movies 3, 4). Thus, the presence of actin foci correlates with the arrested synapses, and their loss accompanies synapse symmetry breaking.

We posited that the loss of actin foci during synapse disengagement may result from WASP downregulation since the actin foci in the synapse are nucleated by WASP[30] and TCR signaling-induced degradation of WASP has been reported previously[53, 54, 55]. Consistent with this idea, we detected a sizeable reduction in total as well as active forms of WASP (phospho-Y293) at 20' post T cell activation in the T cell-substrate interface by TIRF microscopy as well as at the whole cell level by western blotting (Fig. 2c, d). Forced overexpression of WASP at late times by transient expression of GFP-tagged WASP in T cells (Supp. fig. 5a) rescued foci and synapse symmetry (Supp. fig. 5b) indicating that WASP levels are a fundamental determinant of actin foci and synapse symmetry. Simultaneously, highly dynamic lateral protrusions and retractions at the cell periphery (lamellar fluctuations)[22] occur throughout the duration of a stable synapse (Fig. 2e, Movies 4, 5). Comparison of foci and lamellar dynamics showed that foci had a mean half-life ~3 times longer than the lamellar actin fluctuations in WT cells (Fig. 2e). In WASP$^{-/-}$ cells lacking foci, lamellar fluctuations dominated the overall F-actin dynamics at the synapse (Fig. 2f, Movie 6), as expected. Thus, even during the stable phase of the arrested

bioRxiv preprint doi: https://doi.org/10.1101/437236; this version posted October 8, 2018. The copyright holder for this preprint (which was not certified by peer review) is the author/funder, who has granted bioRxiv a license to display the preprint in perpetuity. It is made available under aCC-BY-NC-ND 4.0 International license.

synapse, actin polymerization drives constant lamellar fluctuations in the periphery that could drive symmetry breaking[39, 56], while actin foci are dynamically nucleated across the interface.

Synaptic actin foci dynamics and associated traction forces support synapse symmetry

We previously demonstrated that actin foci are maintained via continuous nucleation of actin filaments at TCR microclusters[30], a process that can generate localized mechanical stresses[57, 58]. To directly quantify foci-dependent forces in the synaptic contact interface, we employed traction force microscopy (TFM)[59, 60, 61]: T cells were seeded on elastic polyacrylamide gels surface-functionalized covalently with anti-CD3 and ICAM-1 and containing embedded fluorescent beads. Forces exerted by the T cells on the substrate deform the substrate, leading to translocation of beads embedded in the gel from their resting positions (Fig. 3a). Following 5 min of seeding onto the substrates, T cells were acutely detached by addition of EDTA and bead translation during substrate relaxation was measured to calculate forces exerted by the T cells. Using this approach, we found that WT T cells exerted substantial forces on the substrate (Fig. 3a). These forces were greatly diminished in WASP$^{-/-}$ cells lacking actin foci (Fig. 3a).

The association of foci with mechanical stresses in the synapse was further reflected in their localization with the phosphorylated form of the mechanosensory protein CasL (pCasL). CasL is recruited to TCR microclusters in T cells upon antigenic stimulation, and undergoes a conformational change allowing phosphorylation of a cryptic N-terminal domain in response to local cytoskeletal stretching[62] (Supp. fig. 6a). In activating T cells, pCasL significantly localized with a TCR signalosome marker- the phosphorylated form of Zap70 (pZap70) along with actin foci (Fig. 3c, Supp. fig. 6b, c), and was reduced by the actin cytoskeleton-disrupting agent latrunculin A (Supp. fig. 6d), as expected for cytoskeletal tension-dependent phosphorylation of CasL. WASP$^{-/-}$ T cells lacking actin foci showed lower levels of pCasL in the interface (Fig. 3c), and at late times, polarizing WT T cells also showed lower pCasL levels (Supp. fig. 6e), indicating lower cytoskeletal stresses in these cells. Furthermore, even though WASP$^{-/-}$ cells adhered and showed the same initial spreading kinetics and symmetrical morphology as WT T cells (Supp. fig. 7a; Movie 7), they formed unstable synapses with much earlier polarization and resumption of motility compared to WT cells (Supp. fig. 7b; Movies 8-10). The instability in WASP$^{-/-}$ synapses was not due to grossly perturbed antigen receptor signaling: various key features of early TCR signaling such as phosphorylation of early TCR signalosome molecules Zap70, LAT and SLP76, and even the recruitment of CasL to the synapse were preserved in WASP$^{-/-}$ cells (Supp. fig. 8a-c). Further, unstable WASP$^{-/-}$ synapses were also not due to reduced integrin signaling, as WASP$^{-/-}$ cells did initially engage ICAM-1 in their synaptic interface and

bioRxiv preprint doi: https://doi.org/10.1101/437236; this version posted October 8, 2018. The copyright holder for this preprint (which was not certified by peer review) is the author/funder, who has granted bioRxiv a license to display the preprint in perpetuity. It is made available under aCC-BY-NC-ND 4.0 International license.

recruited normal amounts of talin (Supp. fig. 9a). Furthermore, treatment with $MnCl_2$[47] (Supp. fig.9b) or supplementation of cytoplasmic Ca^{2+} levels using acute treatment with the thapsigargin[63] (Supp. fig.10a-b) did not block the early polarization of $WASP^{-/-}$ cells, indicating that integrin activation and calcium signaling are insufficient to reconstitute synapse symmetry in these cells. However, a restoration of actin foci and synapse symmetry could be observed when GFP-WASP was transiently overexpressed in WASP-deficient T cells (Supp. fig.11a-c).

To discount the possibility that lower mechanical stress in the interface and faster synapse symmetry breaking in $WASP^{-/-}$ cells was an artifact of the minimal activation surfaces used here, or is a feature specific to murine T cells, we utilized $CD4^+$ T cells derived from human WAS patient cells activated using live antigen presenting cells. Similar to the case of the murine cells (Supp. fig. 12a), WAS cells showed poor mechanotransduction, whether activated on anti-CD3/ICAM-1-coated coverslips (Supp. fig. 12b) or APCs (Fig. 3d, Supp. fig. 13a), and broke synapses more frequently, even though the total F-actin content was normal. Faster synapse symmetry breaking in WAS cells was also not due to a developmental defect, since transient reduction in WASP in healthy human T cells using short-hairpin RNA (shRNA)[30] yielded similar defects in pCasL and symmetry as seen with WAS cells (Supp. fig. 13a). Furthermore, the reduced synaptic pCasL in these cells was due to loss of the actin nucleation-promoting factor (NPF) activity of WASP– overexpression of a WASP construct defective in NPF activity was indistinguishable from total WASP deficiency (Supp. fig. 13b). Together, these data indicate that Lack of foci nucleation underlies premature symmetry breaking in $WASP^{-/-}$ T cells.

In-plane cytoskeletal tension bolstered by actin foci dynamics promotes synapse stability

TFM measurements and pCasL accumulation showed that actin foci are associated with mechanical forces in the synapse. However, traction forces themselves do not explain how foci could promote synapse symmetry, since traction does not necessitate interface symmetry and has the potential to drive contact breaking and cell migration [64]. To further explore the relationship of cytoskeletal forces with synaptic interface symmetry, we next utilized a computational model of the actin cytoskeletal architecture and synaptic interface mechanics. We employed a reductionist Brownian dynamics model of actin dynamics at the cell-substrate interface[65, 66]. This model is based on the distinct behavior of actin foci and Lamella, the two distinct cytoskeletal networks observed at the synapse (Fig. 2e), and incorporated three key differences observed between these actin structures: (i) we model foci as sites with higher actin nucleation rates than the lamella (as measured in [30]), (ii) foci were treated as sites where actin could be immobilized (modeling association with TCR microclusters/integrins) with a lower local unbinding rate than at the lamella (due to the longer lifetime of foci vs. peripheral lamellar fluctuations), and (iii)

bioRxiv preprint doi: https://doi.org/10.1101/437236; this version posted October 8, 2018. The copyright holder for this preprint (which was not certified by peer review) is the author/funder, who has granted bioRxiv a license to display the preprint in perpetuity. It is made available under aCC-BY-NC-ND 4.0 International license.

foci were spatially placed across the synapse compared to the peripheral lamella (Fig. 4a). The T cell contact interface was approximated as an 8 µm square, and a thin volume of the cytoplasm just inside the plasma membrane at the contact was modeled (500 nm thick), mimicking the submembrane actin-rich region[67, 68] (Fig. 4a). Actin foci were modeled as a regular array of 400 nm square sites across the contact plane (small orange squares in Fig. 4a), and the peripheral lamella was modeled as a 400 nm wide zone at each edge of the contact (green); Actin nucleation and actin-linked receptor adhesions to substrate ligands proceed in all of these zones (Fig. 4a). In this framework, F-actin evolves through a series of reactions comprising basic elements of actin dynamics: polymerization/depolymerization/nucleation of actin filaments, actin crosslinking proteins linking/unlinking actin fibers, binding and unbinding of actin filaments to adhesion sites on the substrate, and myosin-mediated contractile forces applied to the cytoskeletal network, with actin nucleation and unbinding rates that differ between each zone.

Simulations of synaptic actin dynamics, cytoskeletal network morphology, and the resultant network tension profile over time were examined under conditions when actin foci are present (modeling wildtype cells; 'WT') or absent (modeling WASP$^{-/-}$ cells). In WT cells, these simulations revealed that actin foci acted as nodes supporting an interconnected actin network across the synaptic interface (Fig. 4b left panels, Movies 11-12). This foci-connected actin network generated and sustained tension across the interface for prolonged durations (Fig. 4c; synaptic stress is a cross-sectional area-normalized measure of the cytoskeletal network tension, parallel to the cell-substrate interface; see 'Methods'), fueled by continual nucleation of filaments at the foci regions and associated myosin contractility (Movies 7, 8). In the absence of actin foci (WASP$^{-/-}$), peripheral lamellae dominate and the F-actin network largely accumulates in a lamella-like distribution (Fig. 4b; Movie 13), accompanied by a relaxation in overall synaptic cytoskeletal tension (Fig. 4b, c). Modeling the late stages of the T cell synapse by first allowing a foci-rich network to form and then downregulating WASP, we saw that loss of WASP from a stable foci-anchored actin network led to rapid dissolution of foci and immediate F-actin redistribution to peripheral lamellar zones, coincident with attenuation of cytoskeletal tension ('WT transitional' Fig. 4b-c, Movie 14).

SIM imaging of F-actin dynamics in the near-interface region of the cytoplasm of live T cells undergoing the transition from the arrested to polarized state confirmed the macroscale changes in the F-actin network suggested by these simulations. In the stable synapse of a WT T cell expressing LifeAct-GFP, inter-foci connections were visible (Fig. 4d '0 sec'). Both foci and their actin interconnections were lost as the cells polarized and regained motility (Insets, Fig. 4d). These results suggest that when foci are present, a restraining tension within the actomyosin network is sustained and supported by foci, across the contact area. Without foci, F-actin is depleted from the central zone and largely enriched in the peripheral lamella, along with myosin activity, as expected in

bioRxiv preprint doi: https://doi.org/10.1101/437236; this version posted October 8, 2018. The copyright holder for this preprint (which was not certified by peer review) is the author/funder, who has granted bioRxiv a license to display the preprint in perpetuity. It is made available under aCC-BY-NC-ND 4.0 International license.

adherent cells poised to break symmetry [27, 69]. It is important to note that while it is the persistent lamellar protrusion that eventually would likely drive motility when symmetry is broken and synaptic stress is low [27, 69], we could not model the protrusions in our simulations since experimentally measuring boundary adhesion dynamics in primary T cells is technically limited. Together, these simulations suggest that actin foci serve as nodes for tension generation within the synapse, which may contribute to their role in sustaining synapse symmetry.

Synaptic tension required for synapse stability is generated by an interplay of actin foci and myosin II activity

In the computational model, myosin II contractile activity played a major role in generating cytoskeletal network tension across the synapse. Since local intracellular cytoskeletal tension dynamics are difficult to measure experimentally, we instead tested the role of myosin-mediated tension generation via acute pharmacological perturbations of myosin II to uncouple actin foci from myosin-mediated tension generation. Inhibition of myosin II using Blebbistatin (Blebb.) led to reduced pCasL levels and premature T cell polarization, even though foci and talin accumulation in the interface were not reduced (Fig. 5a-c). Thus, myosin II functions downstream of foci to generate cytoskeletal contractile tension, and loss of this mechanical tension promotes T cell polarization. pCasL levels in Blebb.-treated cells were not as low as in WASP$^{-/-}$ cells, which may reflect residual cytoskeletal stresses arising from actin polymerization at the actin foci[30, 57]. Blebb. treatment also did not further exacerbate the tendency of WASP$^{-/-}$ T cells to break symmetry, as expected in our model (Fig. 5d-e). Cells treated with the Arp2/3 complex inhibitor CK666 that preferentially ablates foci[30], were included as a control, demonstrating that pharmacological inhibition of actin foci results in reduced pCasL and an increased tendency for T cell polarization (Fig. 5b-d, Movie 15).

To further examine if the synapse-wide transmission of foci-dependent cytoskeletal tension is important for maintenance of a symmetric synapse, we carried out simulations of the actin network as in Fig. 3, where we allowed the actin network to evolve for 120 seconds, and then selectively ablated F-actin network connectivity and tension in a spatially controlled manner (dashed area in the simulation snapshot of Fig. 5e). This was achieved using localized myosin II inactivation and crosslinking of associated F-actin, and this perturbation was found to cause a disruption in synaptic F-actin organization and symmetry, as well as a significant lowering of overall synaptic tension (Fig. 5f-g, Movie 16). To experimentally test the prediction that the symmetry of F-actin tension is important for synapse maintenance, we utilized a photoreactive form of Blebbistatin (azido-blebb) to optically crosslink the actomyosin network in a spatially controlled manner[70]. Azidoblebb. binds to myosin II, and following excitation with UV light crosslinks the actomyosin network, effectively freezing actomyosin contractions in a

bioRxiv preprint doi: https://doi.org/10.1101/437236; this version posted October 8, 2018. The copyright holder for this preprint (which was not certified by peer review) is the author/funder, who has granted bioRxiv a license to display the preprint in perpetuity. It is made available under aCC-BY-NC-ND 4.0 International license.

spatially-controlled fashion. LifeAct-GFP-expressing T cells forming a symmetric synapse were treated with low doses of azido-blebb, photoactivated locally on one edge of the cell (dashed boxes in Fig. 5h), and imaged under low excitation power to avoid phototoxicity. Photoactivation of the inhibitor induced an immediate deflection of the cellular center of mass and transition to a polarized morphology (Fig. 5h-i, Movies 17, 18). Thus, symmetry maintenance requires tension transmission across the interface, mediated by high filament nucleation at actin foci and myosin contractile activity. The perturbation of this tensional mechanism via loss of foci, myosin II inhibition, or localized actomyosin crosslinking leads to a loss of cellular symmetry (Fig. 6).

Discussion

Transitions in motility states underlie T cell immune function. The fast motility state of T cells is associated with immunosurveillance, while antigen-induced arrest is considered to be a hallmark of activation, both in *in vitro* and *in vivo*[5, 12, 13, 14, 15]. Here, using primary T cells, we have identified and characterized an antigen-induced cytoskeletal tension program that actively prolongs their arrested or 'synaptic' state. Loss of this mechanism, which normally happens when cells are sufficiently activated, leads to an immediate unraveling of the arrested synaptic contact followed by resumption of cellular motility. The experiments presented here reveal the cytoskeletal architectures that T cells utilize to tune mechanical tension within the synapse in order to achieve a rapid shift in motility. These results also further our understanding of the mechanical deficits underlying deficient T cell function in Wiskott-Aldrich syndrome and provide a conceptual framework to assess synaptic organizational defects in other actin-related primary immunodeficiency diseases.

The process underlying immediate arrest of T cells when they encounter APCs displaying high-affinity antigens and concomitant formation of a symmetric contact has classically been termed the "stop signal" in immunology [5, 13, 19, 71, 72, 73]. We find that actin foci are an integral part of the cellular machinery associated with maintaining TCR signaling-induced motility arrest. Previous studies have associated intracellular calcium flux in T cells with the stop signal[2, 19]. While it is intuitive that actin foci machinery would communicate with the calcium stop signal pathway for coordinating synapse stability, it is unclear how this communication might take place. At the cellular level, we find evidence that the calcium pathway depends on WASP-dependent actin foci to promote synapse stability. A rise in intracellular calcium induced by thapsigargin is able to freeze shape transitions only in migrating WT T cells (data not shown). Furthermore, foci-lacking WASP$^{-/-}$ T cells do not arrest when treated with thapsigargin. In contrast, we show that the foci-mediated synapse retention is independent of intracellular calcium because BAPTA treatment did not reduce foci or promote synapse symmetry breaking. However, it is important to note

bioRxiv preprint doi: https://doi.org/10.1101/437236; this version posted October 8, 2018. The copyright holder for this preprint (which was not certified by peer review) is the author/funder, who has granted bioRxiv a license to display the preprint in perpetuity. It is made available under aCC-BY-NC-ND 4.0 International license.

that the methodology we used to examine the foci-intracellular calcium connection using pharmacological calcium elevation can generate minor off-target effects on symmetry and foci, since they alter some basic features of the synapse (e.g. talin downregulation in thapsigargin treatment). Furthermore, a previous study proposed that T cells could selectively utilize actin-based versus calcium-based mechanisms of synapse stability based on antigen affinity[74]. This implies that the calcium or foci-mediated stop-signal pathways could be selectively dominant depending on the strength of the TCR-antigen interaction. Thus, a detailed investigation using live imaging of Ca^{2+} reporters in T cells at high spatio-temporal resolution[75] at varying antigen strengths[74] is warranted before a direct connection between foci and calcium signaling for the 'stop signal' mechanism can be established.

Even though the foci, being F-actin-nucleating structures, might generate protrusive forces perpendicular to the interface, we find that the protrusive behavior of the foci orthogonal to the substrate is not required for lateral synapse stability. Foci-mediated synapse stabilization proceeds regardless of the substrate stiffness and operates even when the substrate is too hard for the foci to protrude into (e.g. glass coverslips). Furthermore, inhibition of myosin predisposes synapses to break under conditions where foci nucleation and thus protrusion is not inhibited. Instead, our data suggests that actin foci act as stakes anchoring a tension-bearing actin network parallel to the interface plane (Fig. 6). Myosin activity generates symmetric cytoskeletal tension throughout this network which we hypothesize counters the protrusive forces of the peripheral lamallae. The anchoring function of foci dominates over lamellar protrusions in part via their longer lifetime, and by virtue of foci being distributed across the synaptic interface. When these two requirements are met, actin foci can feed the actomyosin tensional network and stabilize synapses, irrespective of the substrate stiffness. When T cells are activated by supported lipid bilayers, actin foci are not static but move with TCR microclusters[30]. Yet in this system, the stability of synapse still relies on the presence of foci[21]. The dependence of synapse stability on cell-intrinsic cytoskeletal dynamics rather than the substrate stiffness raises an exciting possibility that T cells could utilize cytoskeletal tension to sustain their synapse, when encountering antigens from APCs of varying stiffness.

The generation of filaments by foci to assemble an actomyosin system that organizes and scales mechanical tension across the contact interface reported here resembles the focal adhesions (FA) reported previously in fibroblasts[76]. However, there is a key difference between the two mechanisms. FAs attach to stable actin filaments. Consequently, a cell can detach from the substrate by generating high forces that overcome tension at the FA and rupture them. In contrast, there is continual nucleation and generation of actin filaments at foci. Under these circumstances, forces of detachment would dissipate at foci and the only way to overcome the foci is to downregulate their formation, which is what we see in cells that are preparing to migrate. In this regard,

bioRxiv preprint doi: https://doi.org/10.1101/437236; this version posted October 8, 2018. The copyright holder for this preprint (which was not certified by peer review) is the author/funder, who has granted bioRxiv a license to display the preprint in perpetuity. It is made available under aCC-BY-NC-ND 4.0 International license.

the foci are a departure from the classical "clutch mechanism" proposed for the FAs[76], and represent an adhesion modality that T cells have evolved for their specialized motility requirements.

The results presented in this study indicate that mechanisms of synapse formation and synapse maintenance are mechanistically distinguishable. While increased F-actin is required for the former, the latter constitutes only a change in F-actin organization and overall F-actin content is constant. Similarly, activation of the integrin LFA1 is a prerequisite for successful synaptic engagement, but is not needed for maintenance of the synapse. These results support a recent finding that the LFA1-ICAM1 interaction is not sufficient for stable CD4 T cell-DC synapses in the lymph node[77]. The physiological implications are that T cells may use integrin-based adhesion to initiate synaptic contacts with selective cellular partners[14, 77], but maintain adhesion using lateral tensional mechanisms within the cell provided by the dynamic cytoskeletal arrangements comprising foci nucleation and acto-myosin contractions described here.

In their lifetime, T cells encounter antigens in diverse mechanical microenvironments. The antigen-induced tensional pathway identified here represents a T cell-intrinsic tool to accommodate mechanical disparities between antigen presenting cells, and achieve optimal antigen sampling time. Different T cell subtypes are known to display varying motilities even when they encounter the same APC type[10], and T cells encounter antigens of varying affinities for their TCRs. How the actin foci-based mechanisms outlined here operate in these diverse contexts remains an open question. Simultaneous examination of the effects of antigen affinity on foci, TCR triggering, and T cell activation in different T cell classes will help establish a relationship between TCR antigen affinity and mechanotransduction via this tensional mechanism at the immunological synapse. Future studies will also clarify the ways in which the described mechanical deficits in the synapses formed by WASP deficient T cells contribute to the WAS immunodeficiency at the whole-organism level[28].

Acknowledgements:

We thank A. Thrasher and D. Cox for WASP constructs, and J. Burkhardt and Nathan Roy for LifeAct-GFP mice. We thank the Advanced Imaging Center at Janelia Campus and J. Haddleston for help with the Lattice Light Sheet microscopy, and the Keck microscopy facility at the Whitehead Institute. We are thankful to F. B. Gertler and A. K. Dhawale for input on the experiments and data analysis. This work was supported in part by the Koch Institute Support (core) Grant P30-CA14051 from the National Cancer Institute. We thank the Koch Institute Swanson Biotechnology Center for technical support, specifically Eliza Vasile for OMX Deltavision microscope. This work was supported by the Ragon Institute of MGH, MIT, and Harvard, the National Institutes of Health grant AI43542 (MLD)

bioRxiv preprint doi: https://doi.org/10.1101/437236; this version posted October 8, 2018. The copyright holder for this preprint (which was not certified by peer review) is the author/funder, who has granted bioRxiv a license to display the preprint in perpetuity. It is made available under aCC-BY-NC-ND 4.0 International license.

and Wellcome Trust grant PRF 100262 (MLD), support from Yale University to MM and NIH grant 5R01AI100315 to RG. DJI is an investigator of the Howard Hughes Medical Institute.

Methods:

Cells and reagents:

For most experiments, unless otherwise mentioned, mouse primary $CD4^+$ T cells were isolated from C57BL6/j WT or WASP-/- Mice lymph organs, using EasySep™ Mouse CD4+ T Cell Isolation Kit (StemCell). Cells were rested at 37°C for few hours in culture media (RPMI+ 10%FBS+ 100µM β-merceptoethanol + 1mM Sodium Pyruvate), and used for experiments thereafter. For live imaging, cells were cultured in phenol red free XVivo-10 media (Lonza) supplemented with 10units/ml IL-2. For antigen-specific $CD4^+$T cells, $CD4^+$ T cells were isolated from OTII WT or WASP-/- animals, using the procedure as described above.

For isolating human CD4+T cells, human peripheral blood from healthy donors was acquired from the New York Blood Bank, or from WAS patients at Boston Children's hospital (two patients, males). The blood samples were and transported, handled and processed in accordance with the OSHA guidelines. The cells were isolated from the blood using the $CD4^+$ rosette sep. kit, rested at 37°C in culture media for a few hours and were used in the experiments thereafter.

Unless otherwise mentioned, the inhibitors were purchased from Sigma chemicals, and were used at a concentration indicated in the figure legends. The antibodies for immunostaining including phopho-Y249Cas (#4014), phosphor-Y171 Lat (#3581), phospho-Y397HS1 (clone D12C1), phosphor-Y139/SykY352 Zap70 (clone 65E4) were purchased from Cell Signaling Technology. Anti-phospho-Y145 (#EP2853Y, Novus), anti-tubulin (F2168, Sigma), anti-MyosinII (PRB440P, Covance), anti-WASP (Chicken polyclonal for immunostaining, #Gw22608, Sigma), anti-WASP (Rabbit polyclonal for immunostaining, #SAB4503087, Sigma), anti-phospho Y290 WASP (#Ab59278, Abcam), and anti-Talin (clone C20, Santacruz), were purchased from the indicated vendors.

Cell activation substrates:

In most experiments glass coverslip (#1.5 chambered coverglass, Thermo Scientific) coated with 10ug/ml anti-CD3 and 1 µg/ml ICAM1 were used as activating substrate. For cell-cell conjugate experiments, either IFNγ (100units/ml, overnight)- treated and superantigen loaded HUVEC cells [30], or antigen-loaded, differentiated primary BMDCs were used for synapse assays with human or mouse T cells respectively. In experiments examining the distribution of ICAM1 on activating substrates, planar lipid bilayer system was used. Glass-supported lipid bilayers were deposited

bioRxiv preprint doi: https://doi.org/10.1101/437236; this version posted October 8, 2018. The copyright holder for this preprint (which was not certified by peer review) is the author/funder, who has granted bioRxiv a license to display the preprint in perpetuity. It is made available under aCC-BY-NC-ND 4.0 International license.

and were reconstituted with anti-CD3-Alexa568, and ICAM1X12-his- cy5, and incubated with T cells as described previously [30].

M**icroscopy:**

Interference Reflection Microscopy: For IRM, LabtekII chambers were coated with anti-CD3 and ICAM1, were washed and incubated with the $CD4^+$T cells suspended in the growth media. Care was taken to maintain the temperature of the T cells to 37°C, between the transfers from the culture dish to imaging chambers. The chambers were imaged using a temperature controlled 37°C stage adaptor on a Zeiss LSM510 confocal microscope equipped with a 63X 1.40 NA objective. The samples were imaged using the 543nm Laser at 0.1mW, and collected using Zeiss LSM software. Images were analyzed using Fiji Software.

Structured illumination microscopy: For SI superresolution microscopy, fixed cells were imaged with an OMX-3D microscope, V3 type (Applied Precision, GE), equipped with 405-, 488-, and 594-nm lasers and three Photometrics Cascade II EMCCD cameras. Images were acquired with a 100×, NA 1.4 oil objective at 0.125-µm Z steps using 1.518 immersion oil at room temperature. The images were acquired under the same illumination settings across the individual experiment and then processed with OMX SoftWoRx software (Applied Precision, GE). Images were saved in the TIFF format after reconstruction and alignment using optimized OTFs and wiener filter settings. The images reconstructed using SIM SoftWoRx processing software and were then analyzed using Image J.

TIRF: For the TIRF experiments, a Nikon revolution spinning disc confocal system equipped with a TIRF module and Andor iXON EMCCD camera was used. The images were acquired using 405nm, 488nm, 561nm, and 642nm lasers, a 100X objective (NA 1.49) and a 1.5X projection lens, and analyzed using Fiji software. The depth of TIRF field was maintained to 120nm- 200nm, as measured by optically resolved fluorescent beads.

Confocal Microscopy and azidoblebbistatin experiment: For imaging cell-cell conjugates, Nikon revolution spinning disc confocal microscope equipped with Yokagawa CSU-X1 module was used. Images were acquired using 100X objective (NA 1.49) along with a 1.5X projection and an Andor iXON EMCCD camera. For azidoblebbistatin treatment experiment, the above mentioned spinning disc system was used to acquire a 0.4um optical section in the plane of the synapse, coupled with live microscopy. Cells were allowed to form synapses, and were treated with either inhibitor or DMSO just before imaging. During imaging, the inhibitor was activated by excitation with 5 brief pulses of 405nm laser at 50mW power employing the Andor FRAPPA photomanipulation system. Images were subsequently analyzed using Fiji software and plotted using MATLAB software.

bioRxiv preprint doi: https://doi.org/10.1101/437236; this version posted October 8, 2018. The copyright holder for this preprint (which was not certified by peer review) is the author/funder, who has granted bioRxiv a license to display the preprint in perpetuity. It is made available under aCC-BY-NC-ND 4.0 International license.

Lattice light sheet: The lattice light sheet microscope (LLSM) used in these experiments is housed in the Advanced Imaged Center (AIC) at the Howard Hughes Medical Institute Janelia research campus. The system is configured and operated as previously described[52]. Briefly, T cells were activated on 5mm round glass coverslips (Warner Instruments, Catalog # CS-5R), plasma-treated and coated with anti-CD3 and ICAM1-extracellular domain, and imaged in culture media at 37°C. Samples were illuminated by lattice light-sheet using 488 nm diode lasers (MPB Communications) through an excitation objective (Special Optics, 0.65 NA, 3.74-mm WD). Fluorescent emission was collected by detection objective (Nikon, CFI Apo LWD 25XW, 1.1 NA), and detected by a sCMOS camera (Hamamatsu Orca Flash 4.0 v2). Acquired data were de-skewed as previously described [52] and deconvolved using an iterative Richardson-Lucy algorithm. Point-spread functions for deconvolution were experimentally measured using 200nm tetraspeck beads adhered to 5 mm glass coverslips (T7280, Invitrogen) for 488 excitation wavelength.

Traction force measurements: Cell root-mean-square (RMS) tractions at the basal surface were quantified by measuring embedded fluorescent submicrometer particle displacement fields in the gel substrates, following published methods[60]. Briefly, carboxylated red fluorescent submicron beads (0.2 µm in diameter; F-8810, Life Technologies) were embedded in the hydrogel substrates, the substrates were then covalently functionalized with anti-CD3 (2C11, 10µg/ml) and ICAM-1-12XHis (2µg/ml). Cells were seeded at a concentration of 2 million/ml and allowed to adhere at 37°C for 5 min before the traction force was measured. The un-adhered cells were removed by gentle aspiration with warm culture media before imaging the cells and beads. Fluorescence images of the microbeads were taken using Olympus FV1200 laser scanning confocal system equipped with 30X silicone oil objective (1.05NA), and 550nm laser line, both when the cells were adhered, and again after cells were removed from the substrate using EDTA. Using a custom Matlab code, the displacement of the fluorescent beads at the apical surface of the hydrogel were computed. The RMS traction generated by the cell was calculated based on the displacement field and the known stiffness of the hydrogel substrate. The substrate stiffness of the hydrogel was 100 kPa, prepared using published protocols[59, 61].

Brownian Dynamics Model of Active Actin Networks during T-cell Activation

We simulated cytoskeletal networks that consist of actin filaments that can polymerize, depolymerize, and nucleate; actin crosslinking proteins (ACPs) that can bind and unbind in a force-sensitive manner; and active myosin II motors that walk along actin filaments generating tension. The model is based on Brownian dynamics and described in detail in our previous work with no inertia[65, 66]:

bioRxiv preprint doi: https://doi.org/10.1101/437236; this version posted October 8, 2018. The copyright holder for this preprint (which was not certified by peer review) is the author/funder, who has granted bioRxiv a license to display the preprint in perpetuity. It is made available under aCC-BY-NC-ND 4.0 International license.

$$\boldsymbol{F}_i - \zeta_i \frac{d\boldsymbol{r}_i}{dt} + \boldsymbol{F}_i^T = 0$$

Where, $\boldsymbol{Fi}$ is the deterministic force determined by the elasticity of the network; $\boldsymbol{\zeta i}$ is the drag of the medium; $\boldsymbol{Fi}$^$\boldsymbol{T}$- stochastic thermal force; and $\boldsymbol{ri}$ – is the position of *i* th particle.

The equation is evolved via Euler's method and solved over time. Extensive details and parameter values, most of which are based on experimental data, of all features in our model can be found here[66]. Supp. table 1 provides parameter values used in this study in order to investigate the spatial and temporal modulations of the actin cytoskeleton to mimic actin foci formation in the synapse during T cell activation. Cytoskeletal network stresses (in the stress profile plots) are calculated by summing the normal component of tensional forces acting on cytoskeletal components across x-z and y-z cross-sections, divided by the cross-section areas.

To model the T-cell synapse formed against a flat surface, we simulated a thin 3D domain (8 µm x 8 µm x 0.5 µm) with active cytoskeletal components. In this domain, we defined regions with different local kinetics of dynamic cytoskeletal components. At the edges of the cell (400nm width from each edge in the x and y directions), to mimic the integrin-rich peripheral lamella which is important in cell migration, adhesions between actin and the bottom surface are enabled. In the middle of the cell to mimic foci mediated adhesions, a 5 x 5 grid of sites each 400 x 400 nm^2 enables adhesions between actin filaments and the bottom surface. No boundary adhesions are enabled in other parts of the domain. The nucleation rate of actin filaments is highest at the foci region. To mimic azidoblebbistatin treatment in our simulations, at 100s after the activation of myosin motor walking, we deactivated motor walking and actin-to-substrate adhesions at the top 40% of the domain.

Fig. 4A shows the spatial profile of the kinetics of actin nucleation and adhesion used for simulations, and Supp. table 1 shows the parameter values used for the simulations. Because exact rates controlling actin dynamics in live cells are elusive due to the plethora of actin regulating factors (formins, Arp2/3, cofilin, capping proteins, etc.) and spatiotemporal biochemical signaling (e.g. via Rho GTPases), we chose rates of actin turnover comparable to experimental observations [78] and probed idealized spatial profiles that can capture the spatial distributions of actin seen in T-cells during activation.

Image analysis and statistics

The images were analyzed using Fiji software. For determination of cell shape (AR), automated cell boundaries were creating by first thresholding the actin images to remove background, watershed plugin to fill the low

bioRxiv preprint doi: https://doi.org/10.1101/437236; this version posted October 8, 2018. The copyright holder for this preprint (which was not certified by peer review) is the author/funder, who has granted bioRxiv a license to display the preprint in perpetuity. It is made available under aCC-BY-NC-ND 4.0 International license.

intensity areas within the cell areas created by threshold operation, and finally with 'analyze particles' utility of Fiji. Using the automated boundaries, the raw images were analyzed for the intensity of relevant proteins within each synapse. Foci were estimated as described previously[30]. Briefly, a moving window of 1.6X1.6 μm^2 was used to create a Gaussian blur image of the original raw images. The Gaussian blur image was subtracted from the raw image to create the foci image. Data was plotted using Graphpad Prism or MATLAB. For statistical analysis, Mann-Whitney non-parametric two-tailed test was performed to compare population of cells. In all graphs, unless otherwise mentioned, the dataset was normalized to the mean values of the 'Control' population, and then plotted as a 'normalized' value. Most graphs highlight the Mean ± SEM in the scatter plot of normalized values, where each dot represents values obtained from a single cell, unless otherwise mentioned.

bioRxiv preprint doi: https://doi.org/10.1101/437236; this version posted October 8, 2018. The copyright holder for this preprint (which was not certified by peer review) is the author/funder, who has granted bioRxiv a license to display the preprint in perpetuity. It is made available under aCC-BY-NC-ND 4.0 International license.

Figure Legends:

Figure 1. Synapse polarization involves actin remodeling in T cells and proceeds despite of integrin augmentation. (a) General schematic of the assay system used in this study for examining the process of synapse sustenance vs. polarization, post initial T cell adhesion and spreading on the antigen presenting surface (APS). Cell-APS interface of T cells was imaged for synapse establishment and maturation (5') and eventual symmetry breaking and polarization (20'). (b-d) T cell interface actin re-organization during synapse symmetry breaking, imaged using SIM. (b) Quantification of the shape, or, relative fluorescence signal of the indicated proteins in the SIM images (c, d), normalized to levels detected at 5'; points represent values for individual cells. p values are: ** =0.003 for foci, **= 0.008 for talin, and p =0.36 for total F-actin using Mann-Whitney two-tailed test. (e-f) Integrin augmentation does not rescue synapse symmetry breaking. Cells were allowed to adhere to the APS for 5' or 10', and were then treated with vehicle control, 0.5mM $MnCl_2$ or 100nM A286982 for subsequent 10'. Cells were fixed, stained and imaged using SIM (e) and analyzed for shape change (e) as well as talin recruitment, F-actin and foci at the synapse (f). p values in the graph, n.s. > 0.05; *** <0.001; *= 0.01; **<0.009.

Figure 2. Synapse symmetry involves temporal regulation of WASP and WASP-dependent actin dynamics. (a)Time-lapse imaging of LifeAct-GFP expressing T cell using Lattice lightsheet microscopy (LLSM) during synapse polarization. Shown are snapshots at selected timepoints (left) and a kymograph of actin foci (denoted by arrows in the first image panel) over time (right) for a representative T cell. (b) Quantification of changes in actin foci and cellular aspect ratio in LLSM images during symmetry breaking. (c) T cells incubated with APS for the indicated time periods were processed for immunostaining (c) or for western blotting (d). Graph in (c) shows relative levels of total and active WASP (WASP-phosphorylated at Y293, pWASP), normalized to the mean levels at 5'. Numbers at the bottom of the western blot in (d) indicates WASP band intensity divided by the actin band intensity, and resulting ratios normalized to the values at the 0' time point (non-activated cells). (e-f) Actin dynamics in mature synapse of LifeAct-GFP expressing T cell using TIRFM. The images show the foci (pseudocolored red) extracted from the total synaptic F-actin, and kymograph shows the time course of foci and lamellar activity over a period of 210 sec. Histograms of foci and lamellar protrusion and retraction (fluctuations) dynamics in WT T cell (e); Lifetime of individual foci and lamellar events (graph on the bottom right, each dot represents a single foci/lamellar protrusion-retraction event). ***<0.0001 using Mann-Whitney two-tailed test. (f) Shows a kymograph of the lamellar activity of WASP-deficient cells that lack actin foci.

bioRxiv preprint doi: https://doi.org/10.1101/437236; this version posted October 8, 2018. The copyright holder for this preprint (which was not certified by peer review) is the author/funder, who has granted bioRxiv a license to display the preprint in perpetuity. It is made available under aCC-BY-NC-ND 4.0 International license.

Figure 3. Foci associated mechanical forces are linked to synapse symmetry.

(a-b) Foci –deficient cells display poor traction forces in their synapse. WT or WASP$^{-/-}$ T cells were incubated on polyacrylamide substrates covalently functionalized with anti-CD3 and ICAM1, and traction force measurements were carried out as described in 'Methods'. The images in the right show traction force maps without (left panels) or with (right panels) force vectors. p value, ***<0.0001. (c) SIM imaging of WT or WASP$^{-/-}$ T cells activated by APS for 5'. The graphs show quantification of actin foci pCasL and talin levels in the synapse (Middle graph); right graph shows AR measurement *** =0.0001; p value for talin =0.07, as determined by the Mann-Whitney two-tailed test. (d) Human WAS patient CD4^{+}T cells- APC conjugates display synapse symmetry defects similar to those observed in mouse WASP$^{-/-}$ CD4^{+} T cells. CD4^{+}T cells purified from healthy controls or WAS patients were incubated with superantigen loaded HUVEC cells for 5' (APC; see 'Methods') and imaged using confocal microscopy. Each image represents a maximum intensity projection of the synaptic area. In the graphs, p values; *** <0.001; n.s. =0.09, as determined by the Mann-Whitney two tailed test.

Figure 4. Computational simulations to explain the cytoskeletal basis of symmetry sustenance at synapse.

(a) Outline of the spatial scheme utilized to simulate synapse cytoskeletal dynamics. Cartoon on the left shows the spatial patterning of the two major actin networks: the lamellar F-actin network in the peripheral zone that would continuously undergo fluctuations, and foci. The foci are interspersed throughout the synapse within a dynamic lamellar F-actin network. The peripheral lamellar fluctuations seen in live imaging could not be included in the simulations due to unavailability of data on fresh boundary adhesions. The cartoon on the right shows square simulation space patterned after the cartoon on the left and utilized here for simulations. The actin nucleation and adhesion parameters used at the foci and lamellar zones are indicated on the right.

(b) Simulation of T cell IS F-actin behavior and resultant mechanical tension incorporating the differential dynamics and positioning of foci and lamella across the synaptic interface, using Brownian dynamics equation with no inertia (see 'Methods'). The images show simulation snapshots at the beginning (0min; soon after the attachment and spreading of T cells on the substrates) and the end of the simulations for the three IS cases – with persistent foci (WT, left most panels), with no foci (WASP$^{-/-}$, middle right panels), and with WASP and consequently foci downregulated after a period of synapse maturation (WT transitional). The colors in the images indicate myosin II motor (pseudocolored teal), F-actin crosslinking proteins (pseudocolored yellow), and the F-actin filaments (pseudocolored blue for the low tension and the red for thigh tension actin filaments); middle left image panels show the distribution of the aforementioned proteins at individual foci site at a higher magnification.

bioRxiv preprint doi: https://doi.org/10.1101/437236; this version posted October 8, 2018. The copyright holder for this preprint (which was not certified by peer review) is the author/funder, who has granted bioRxiv a license to display the preprint in perpetuity. It is made available under aCC-BY-NC-ND 4.0 International license.

(c) Predicted stress (tension normalized to the area) profiles within the cytoskeletal architecture as the synaptic contact progresses in time, corresponding to the three cases shown in b. (d) Live imaging of a T cell using SIM shows the inter-foci connections (arrows in the inset) as predicted in the simulations; and their loss concomitant with loss of actin foci, as the T cell polarizes to initiate motility (compare insets between 0 and 120 sec). '0 sec' refers to the beginning of the observation of the cell, after it has attached to the substrate, spread and maintained synapse for 12min.

Figure 5. Pharmacological interrogation of actin foci-myosin crosstalk in sustaining symmetry.

(a) Schematic of the cytoskeletal inhibitors and their targets used in the experiments.

(b-e) SIM imaging of mouse T cells activated for 5' on APS, then treated with the indicated inhibitors or vehicle control. Shown are the representative SIM images (b), and quantification of actin foci, talin, or pCasL in the contact interface (normalized to control cells, c), and measured cell morphology aspect ratios (d,e). Since CK666 treatment reduces F-actin intensity[30], the 'actin' image of the CK666 treated cell in (b) was contrasted differently than the 'control' and 'Blebb.' cases for a clearer visualization of F-actin. p values, * =0.02, ** =0.001, n.s. >0.05. For the rest of the comparisons between the control and treatment cases, p <0.0001. For the bar graph in (b), at least 83 cells were used in each case; *p value* for the n.s. cases is 0.05, * =*0.02*. Within the foci, pCasL and talin groups, wherever not shown, the values between the Control and treatment is <0.0001 using Mann-Whitney two-tailed test.

(f-g) Simulation of synaptic F-actin network following localized myosin inactivation and inactivated myosin-mediated F-actin cross-linking within the area marked with dotted line in the left image. The graph shows the predicted alteration in mechanical stress profile, as myosin is inactivated crosslinked in the defined region (marked by an arrow), (g).

(h-i) Experimental confirmation of localized actomyosin crosslinking and symmetry breaking. LifeAct-GFP expressing T cells were incubated with activating substrates, treated with vehicle control or 1 µM Azido-blebb and their contact interface imaged using low excitation laser power (0.5 mW), using a spinning disc confocal microscope (h). The montage shows the shape change and movement that synapse undergoes after it is exposed to a brief flash of blue light crosslinking Azido-Blebb and actomyosin network within the illuminated area (shown with a box in the image). The deflection in center of mass (COM) within a minute was calculated and plotted for at least 10 cells in each case (graphs in h). The left graphs in (i) show individual COM trajectory, and the graph on the right shows average COM movement across cells within a minute post photo-inactivation of myosin II and network crosslinking.

bioRxiv preprint doi: https://doi.org/10.1101/437236; this version posted October 8, 2018. The copyright holder for this preprint (which was not certified by peer review) is the author/funder, who has granted bioRxiv a license to display the preprint in perpetuity. It is made available under aCC-BY-NC-ND 4.0 International license.

Figure 6. Model outlining the mechanistic basis of T cell synapse maintenance. The model argues that in highly migratory T cells, after adhesion and synapse formation, lamellar fluctuations would constantly attempt to break the synapse. An antigen- induced actin foci and associated actomyosin arrangement would generate high in-plane cytoskeletal tension that actively restrains synapse breaking. Via nucleation of actin foci, WASP acts as a central regulator of this mechanism. Downregulation of WASP following T cell activation leads to loss of foci-dependent actin architecture and internal tension resulting into unraveling of the synapse, as is also seen in WASP –deficient cells that are predisposed to synapse symmetry breaking. Images shown at the bottom are the platinum replica electron micrographs of T cell synapses showing actin foci-dependent interconnected cytoskeletal architecture that sustains synapse symmetry in WT T cells (left), and is lacking in WASP-/- T cells (right).

References

1. Grakoui, A. *et al.* The immunological synapse: a molecular machine controlling T cell activation. *Science* **285**, 221-227 (1999).

2. Negulescu, P.A., Krasieva, T.B., Khan, A., Kerschbaum, H.H. & Cahalan, M.D. Polarity of T cell shape, motility, and sensitivity to antigen. *Immunity* **4**, 421-430 (1996).

3. Miller, M.J., Wei, S.H., Parker, I. & Cahalan, M.D. Two-photon imaging of lymphocyte motility and antigen response in intact lymph node. *Science* **296**, 1869-1873 (2002).

4. Dustin, M.L. Hunter to gatherer and back: immunological synapses and kinapses as variations on the theme of amoeboid locomotion. *Annual review of cell and developmental biology* **24**, 577-596 (2008).

5. Mempel, T.R., Henrickson, S.E. & Von Andrian, U.H. T-cell priming by dendritic cells in lymph nodes occurs in three distinct phases. *Nature* **427**, 154-159 (2004).

6. Bajenoff, M. *et al.* Stromal cell networks regulate lymphocyte entry, migration, and territoriality in lymph nodes. *Immunity* **25**, 989-1001 (2006).

7. Stoll, S., Delon, J., Brotz, T.M. & Germain, R.N. Dynamic imaging of T cell-dendritic cell interactions in lymph nodes. *Science* **296**, 1873-1876 (2002).

bioRxiv preprint doi: https://doi.org/10.1101/437236; this version posted October 8, 2018. The copyright holder for this preprint (which was not certified by peer review) is the author/funder, who has granted bioRxiv a license to display the preprint in perpetuity. It is made available under aCC-BY-NC-ND 4.0 International license.

8. Germain, R.N., Robey, E.A. & Cahalan, M.D. A decade of imaging cellular motility and interaction dynamics in the immune system. *Science* **336**, 1676-1681 (2012).

9. Bousso, P. & Robey, E. Dynamics of CD8+ T cell priming by dendritic cells in intact lymph nodes. *Nature immunology* **4**, 579-585 (2003).

10. Tadokoro, C.E. *et al.* Regulatory T cells inhibit stable contacts between CD4+ T cells and dendritic cells in vivo. *The Journal of experimental medicine* **203**, 505-511 (2006).

11. Miller, M.J., Wei, S.H., Cahalan, M.D. & Parker, I. Autonomous T cell trafficking examined in vivo with intravital two-photon microscopy. *Proceedings of the National Academy of Sciences of the United States of America* **100**, 2604-2609 (2003).

12. Celli, S., Lemaitre, F. & Bousso, P. Real-time manipulation of T cell-dendritic cell interactions in vivo reveals the importance of prolonged contacts for CD4+ T cell activation. *Immunity* **27**, 625-634 (2007).

13. Hugues, S. *et al.* Distinct T cell dynamics in lymph nodes during the induction of tolerance and immunity. *Nature immunology* **5**, 1235-1242 (2004).

14. Zaretsky, I. *et al.* ICAMs support B cell interactions with T follicular helper cells and promote clonal selection. *The Journal of experimental medicine* **214**, 3435-3448 (2017).

15. Skokos, D. *et al.* Peptide-MHC potency governs dynamic interactions between T cells and dendritic cells in lymph nodes. *Nature immunology* **8**, 835-844 (2007).

16. Fooksman, D.R. *et al.* Functional anatomy of T cell activation and synapse formation. *Annu Rev Immunol* **28**, 79-105 (2010).

17. Comrie, W.A. & Burkhardt, J.K. Action and Traction: Cytoskeletal Control of Receptor Triggering at the Immunological Synapse. *Frontiers in immunology* **7**, 68 (2016).

18. Martin-Cofreces, N.B. & Sanchez-Madrid, F. Sailing to and Docking at the Immune Synapse: Role of Tubulin Dynamics and Molecular Motors. *Frontiers in immunology* **9**, 1174 (2018).

19. Dustin, M.L., Bromley, S.K., Kan, Z., Peterson, D.A. & Unanue, E.R. Antigen receptor engagement delivers a stop signal to migrating T lymphocytes. *Proceedings of the National Academy of Sciences of the United States of America* **94**, 3909-3913 (1997).

bioRxiv preprint doi: https://doi.org/10.1101/437236; this version posted October 8, 2018. The copyright holder for this preprint (which was not certified by peer review) is the author/funder, who has granted bioRxiv a license to display the preprint in perpetuity. It is made available under aCC-BY-NC-ND 4.0 International license.

20. Wei, X., Tromberg, B.J. & Cahalan, M.D. Mapping the sensitivity of T cells with an optical trap: polarity and minimal number of receptors for Ca(2+) signaling. *Proceedings of the National Academy of Sciences of the United States of America* **96**, 8471-8476 (1999).

21. Sims, T.N. *et al.* Opposing effects of PKCtheta and WASp on symmetry breaking and relocation of the immunological synapse. *Cell* **129**, 773-785 (2007).

22. Roybal, K.T., Sinai, P., Verkade, P., Murphy, R.F. & Wulfing, C. The actin-driven spatiotemporal organization of T-cell signaling at the system scale. *Immunological reviews* **256**, 133-147 (2013).

23. Mullins, R.D. Cytoskeletal mechanisms for breaking cellular symmetry. *Cold Spring Harbor perspectives in biology* **2**, a003392 (2010).

24. Kaizuka, Y., Douglass, A.D., Varma, R., Dustin, M.L. & Vale, R.D. Mechanisms for segregating T cell receptor and adhesion molecules during immunological synapse formation in Jurkat T cells. *Proceedings of the National Academy of Sciences of the United States of America* **104**, 20296-20301 (2007).

25. Babich, A. *et al.* F-actin polymerization and retrograde flow drive sustained PLCgamma1 signaling during T cell activation. *The Journal of cell biology* **197**, 775-787 (2012).

26. Wulfing, C., Sjaastad, M.D. & Davis, M.M. Visualizing the dynamics of T cell activation: intracellular adhesion molecule 1 migrates rapidly to the T cell/B cell interface and acts to sustain calcium levels. *Proceedings of the National Academy of Sciences of the United States of America* **95**, 6302-6307 (1998).

27. Lomakin, A.J. *et al.* Competition for actin between two distinct F-actin networks defines a bistable switch for cell polarization. *Nature cell biology* **17**, 1435-1445 (2015).

28. Thrasher, A.J. & Burns, S.O. WASP: a key immunological multitasker. *Nat Rev Immunol* **10**, 182-192 (2010).

29. Calvez, R. *et al.* The Wiskott-Aldrich syndrome protein permits assembly of a focused immunological synapse enabling sustained T-cell receptor signaling. *Haematologica* **96**, 1415-1423 (2011).

30. Kumari, S. *et al.* Actin foci facilitate activation of the phospholipase C-gamma in primary T lymphocytes via the WASP pathway. *Elife* **4** (2015).

31. Cannon, J.L. & Burkhardt, J.K. Differential roles for Wiskott-Aldrich syndrome protein in immune synapse formation and IL-2 production. *Journal of immunology* **173**, 1658-1662 (2004).

bioRxiv preprint doi: https://doi.org/10.1101/437236; this version posted October 8, 2018. The copyright holder for this preprint (which was not certified by peer review) is the author/funder, who has granted bioRxiv a license to display the preprint in perpetuity. It is made available under aCC-BY-NC-ND 4.0 International license.

32. Henrickson, S.E. *et al.* T cell sensing of antigen dose governs interactive behavior with dendritic cells and sets a threshold for T cell activation. *Nature immunology* **9**, 282-291 (2008).

33. Bohineust, A., Garcia, Z., Beuneu, H., Lemaitre, F. & Bousso, P. Termination of T cell priming relies on a phase of unresponsiveness promoting disengagement from APCs and T cell division. *The Journal of experimental medicine* (2018).

34. Fife, B.T. *et al.* Interactions between PD-1 and PD-L1 promote tolerance by blocking the TCR-induced stop signal. *Nature immunology* **10**, 1185-1192 (2009).

35. Schneider, H. *et al.* Reversal of the TCR stop signal by CTLA-4. *Science* **313**, 1972-1975 (2006).

36. Shulman, Z. *et al.* Dynamic signaling by T follicular helper cells during germinal center B cell selection. *Science* **345**, 1058-1062 (2014).

37. Ridley, A.J. *et al.* Cell migration: integrating signals from front to back. *Science* **302**, 1704-1709 (2003).

38. Fletcher, D.A. & Mullins, R.D. Cell mechanics and the cytoskeleton. *Nature* **463**, 485-492 (2010).

39. Blanchoin, L., Boujemaa-Paterski, R., Sykes, C. & Plastino, J. Actin dynamics, architecture, and mechanics in cell motility. *Physiol Rev* **94**, 235-263 (2014).

40. Bashour, K.T. *et al.* CD28 and CD3 have complementary roles in T-cell traction forces. *Proceedings of the National Academy of Sciences of the United States of America* **111**, 2241-2246 (2014).

41. Hosseini, B.H. *et al.* Immune synapse formation determines interaction forces between T cells and antigen-presenting cells measured by atomic force microscopy. *Proceedings of the National Academy of Sciences of the United States of America* **106**, 17852-17857 (2009).

42. Hu, K.H. & Butte, M.J. T cell activation requires force generation. *The Journal of cell biology* **213**, 535-542 (2016).

43. Lim, T.S., Mortellaro, A., Lim, C.T., Hammerling, G.J. & Ricciardi-Castagnoli, P. Mechanical interactions between dendritic cells and T cells correlate with T cell responsiveness. *Journal of immunology* **187**, 258-265 (2011).

44. Houmadi, R. *et al.* The Wiskott-Aldrich Syndrome Protein Contributes to the Assembly of the LFA-1 Nanocluster Belt at the Lytic Synapse. *Cell Rep* **22**, 979-991 (2018).

bioRxiv preprint doi: https://doi.org/10.1101/437236; this version posted October 8, 2018. The copyright holder for this preprint (which was not certified by peer review) is the author/funder, who has granted bioRxiv a license to display the preprint in perpetuity. It is made available under aCC-BY-NC-ND 4.0 International license.

45. Mayya, V. *et al.* Durable Interactions of T Cells with T Cell Receptor Stimuli in the Absence of a Stable Immunological Synapse. *Cell Rep* **22**, 340-349 (2018).

46. Hons, M. *et al.* Chemokines and integrins independently tune actin flow and substrate friction during intranodal migration of T cells. *Nature immunology* **19**, 606-616 (2018).

47. Dransfield, I., Cabanas, C., Craig, A. & Hogg, N. Divalent cation regulation of the function of the leukocyte integrin LFA-1. *The Journal of cell biology* **116**, 219-226 (1992).

48. Liu, G. *et al.* Discovery of novel p-arylthio cinnamides as antagonists of leukocyte function-associated antigen-1/intracellular adhesion molecule-1 interaction. 1. Identification of an additional binding pocket based on an anilino diaryl sulfide lead. *Journal of medicinal chemistry* **43**, 4025-4040 (2000).

49. Tabdanov, E. *et al.* Micropatterning of TCR and LFA-1 ligands reveals complementary effects on cytoskeleton mechanics in T cells. *Integr Biol (Camb)* **7**, 1272-1284 (2015).

50. Miller, M.J., Safrina, O., Parker, I. & Cahalan, M.D. Imaging the single cell dynamics of CD4+ T cell activation by dendritic cells in lymph nodes. *The Journal of experimental medicine* **200**, 847-856 (2004).

51. Balagopalan, L. *et al.* Plasma membrane LAT activation precedes vesicular recruitment defining two phases of early T-cell activation. *Nature communications* **9**, 2013 (2018).

52. Chen, B.C. *et al.* Lattice light-sheet microscopy: imaging molecules to embryos at high spatiotemporal resolution. *Science* **346**, 1257998 (2014).

53. Macpherson, L. *et al.* Tyrosine phosphorylation of WASP promotes calpain-mediated podosome disassembly. *Haematologica* **97**, 687-691 (2012).

54. Reicher, B. *et al.* Ubiquitylation-dependent negative regulation of WASp is essential for actin cytoskeleton dynamics. *Mol Cell Biol* **32**, 3153-3163 (2012).

55. Watanabe, Y. *et al.* T-cell receptor ligation causes Wiskott-Aldrich syndrome protein degradation and F-actin assembly downregulation. *The Journal of allergy and clinical immunology* **132**, 648-655 e641 (2013).

56. Carvalho, K. *et al.* Actin polymerization or myosin contraction: two ways to build up cortical tension for symmetry breaking. *Philos Trans R Soc Lond B Biol Sci* **368**, 20130005 (2013).

57. Pollard, T.D. & Borisy, G.G. Cellular motility driven by assembly and disassembly of actin filaments. *Cell* **112**, 453-465 (2003).

bioRxiv preprint doi: https://doi.org/10.1101/437236; this version posted October 8, 2018. The copyright holder for this preprint (which was not certified by peer review) is the author/funder, who has granted bioRxiv a license to display the preprint in perpetuity. It is made available under aCC-BY-NC-ND 4.0 International license.

58. Cossart, P. Actin-based motility of pathogens: the Arp2/3 complex is a central player. *Cellular microbiology* **2**, 195-205 (2000).

59. Engler, A.J. *et al.* Myotubes differentiate optimally on substrates with tissue-like stiffness: pathological implications for soft or stiff microenvironments. *The Journal of cell biology* **166**, 877-887 (2004).

60. Poh, Y.C. *et al.* Dynamic force-induced direct dissociation of protein complexes in a nuclear body in living cells. *Nature communications* **3**, 866 (2012).

61. Yeung, T. *et al.* Effects of substrate stiffness on cell morphology, cytoskeletal structure, and adhesion. *Cell motility and the cytoskeleton* **60**, 24-34 (2005).

62. (!!! INVALID CITATION !!! 59, 60, 61).

63. Gouy, H., Cefai, D., Christensen, S.B., Debre, P. & Bismuth, G. Ca2+ influx in human T lymphocytes is induced independently of inositol phosphate production by mobilization of intracellular Ca2+ stores. A study with the Ca2+ endoplasmic reticulum-ATPase inhibitor thapsigargin. *European journal of immunology* **20**, 2269-2275 (1990).

64. Parsons, J.T., Horwitz, A.R. & Schwartz, M.A. Cell adhesion: integrating cytoskeletal dynamics and cellular tension. *Nature reviews. Molecular cell biology* **11**, 633-643 (2010).

65. Kim, T. Determinants of contractile forces generated in disorganized actomyosin bundles. *Biomechanics and modeling in mechanobiology* **14**, 345-355 (2015).

66. Mak, M., Zaman, M.H., Kamm, R.D. & Kim, T. Interplay of active processes modulates tension and drives phase transition in self-renewing, motor-driven cytoskeletal networks. *Nature communications* **7**, 10323 (2016).

67. Fritzsche, M., Lewalle, A., Duke, T., Kruse, K. & Charras, G. Analysis of turnover dynamics of the submembranous actin cortex. *Molecular biology of the cell* **24**, 757-767 (2013).

68. Linsmeier, I. *et al.* Disordered actomyosin networks are sufficient to produce cooperative and telescopic contractility. *Nature communications* **7**, 12615 (2016).

69. Yam, P.T. *et al.* Actin-myosin network reorganization breaks symmetry at the cell rear to spontaneously initiate polarized cell motility. *The Journal of cell biology* **178**, 1207-1221 (2007).

70. Kepiro, M. *et al.* Azidoblebbistatin, a photoreactive myosin inhibitor. *Proceedings of the National Academy of Sciences of the United States of America* **109**, 9402-9407 (2012).

bioRxiv preprint doi: https://doi.org/10.1101/437236; this version posted October 8, 2018. The copyright holder for this preprint (which was not certified by peer review) is the author/funder, who has granted bioRxiv a license to display the preprint in perpetuity. It is made available under aCC-BY-NC-ND 4.0 International license.

71. Downey, J., Smith, A., Schneider, H., Hogg, N. & Rudd, C.E. TCR/CD3 mediated stop-signal is decoupled in T-cells from Ctla4 deficient mice. *Immunol Lett* **115**, 70-72 (2008).

72. Dustin, M.L. T-cell activation through immunological synapses and kinapses. *Immunological reviews* **221**, 77-89 (2008).

73. Dustin, M.L. Regulation of T cell migration through formation of immunological synapses: the stop signal hypothesis. *Adv Exp Med Biol* **512**, 191-201 (2002).

74. Moreau, H.D. *et al.* Signal strength regulates antigen-mediated T-cell deceleration by distinct mechanisms to promote local exploration or arrest. *Proceedings of the National Academy of Sciences of the United States of America* **112**, 12151-12156 (2015).

75. Dong, T.X. *et al.* T-cell calcium dynamics visualized in a ratiometric tdTomato-GCaMP6f transgenic reporter mouse. *Elife* **6** (2017).

76. Kanchanawong, P. *et al.* Nanoscale architecture of integrin-based cell adhesions. *Nature* **468**, 580-584 (2010).

77. Feigelson, S.W. *et al.* ICAMs Are Not Obligatory for Functional Immune Synapses between Naive CD4 T Cells and Lymph Node DCs. *Cell Rep* **22**, 849-859 (2018).

78. Pollard, T.D. Regulation of actin filament assembly by Arp2/3 complex and formins. *Annual review of biophysics and biomolecular structure* **36**, 451-477 (2007).

Figure 1

bioRxiv preprint doi: https://doi.org/10.1101/437236; this version posted October 8, 2018. The copyright holder for this preprint (which was not certified by peer review) is the author/funder, who has granted bioRxiv a license to display the preprint in perpetuity. It is made available under aCC-BY-NC-ND 4.0 International license.

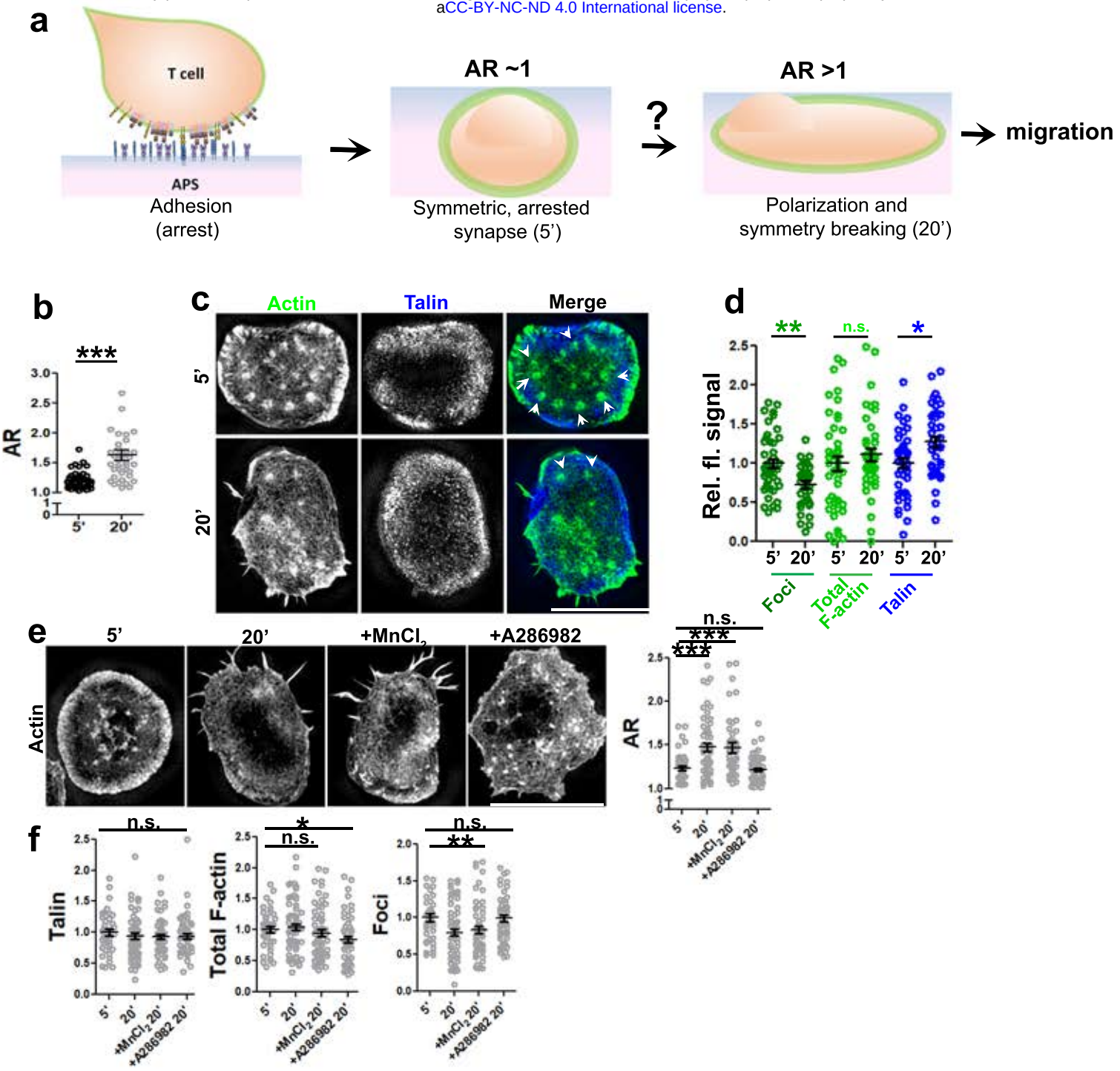

bioRxiv preprint doi: https://doi.org/10.1101/437236; this version posted October 8, 2018. The copyright holder for this preprint (which was not certified by peer review) is the author/funder, who has granted bioRxiv a license to display the preprint in perpetuity. It is made available under aCC-BY-NC-ND 4.0 International license.

Figure 2

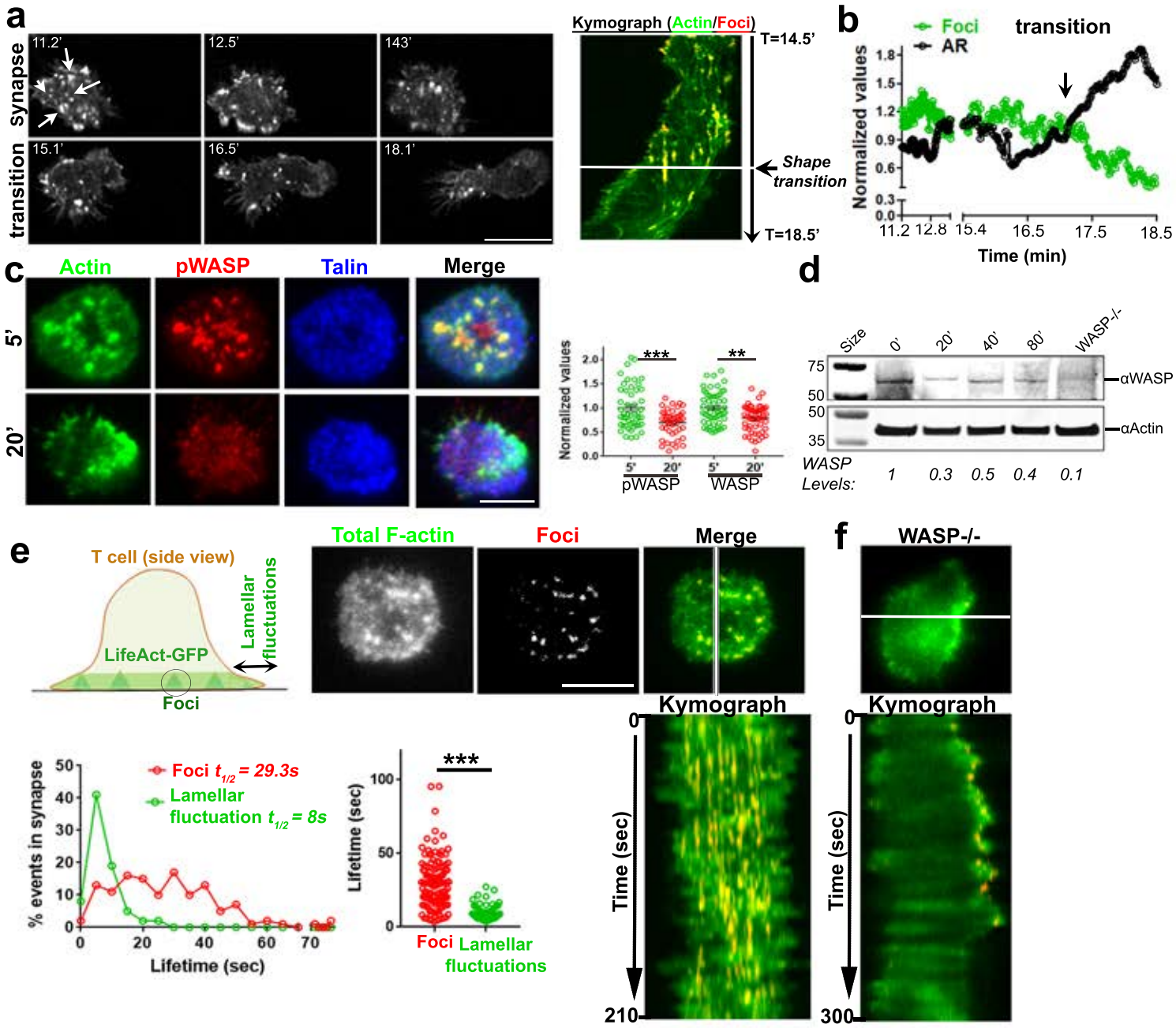

bioRxiv preprint doi: https://doi.org/10.1101/437236; this version posted October 8, 2018. The copyright holder for this preprint (which was not certified by peer review) is the author/funder, who has granted bioRxiv a license to display the preprint in perpetuity. It is made available under aCC-BY-NC-ND 4.0 International license.

Figure 3

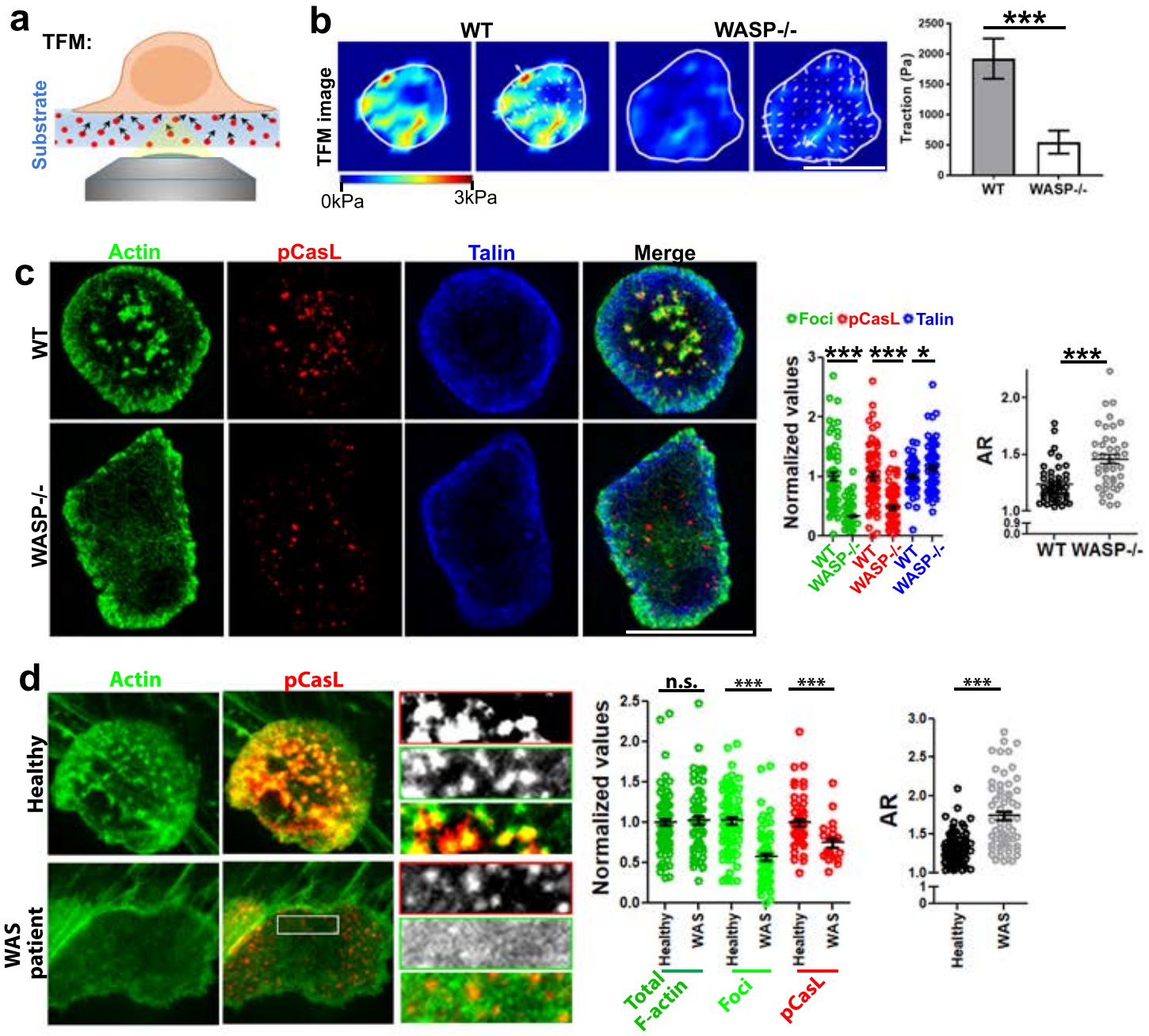

Figure 4

bioRxiv preprint doi: https://doi.org/10.1101/437236; this version posted October 8, 2018. The copyright holder for this preprint (which was not certified by peer review) is the author/funder, who has granted bioRxiv a license to display the preprint in perpetuity. It is made available under aCC-BY-NC-ND 4.0 International license.

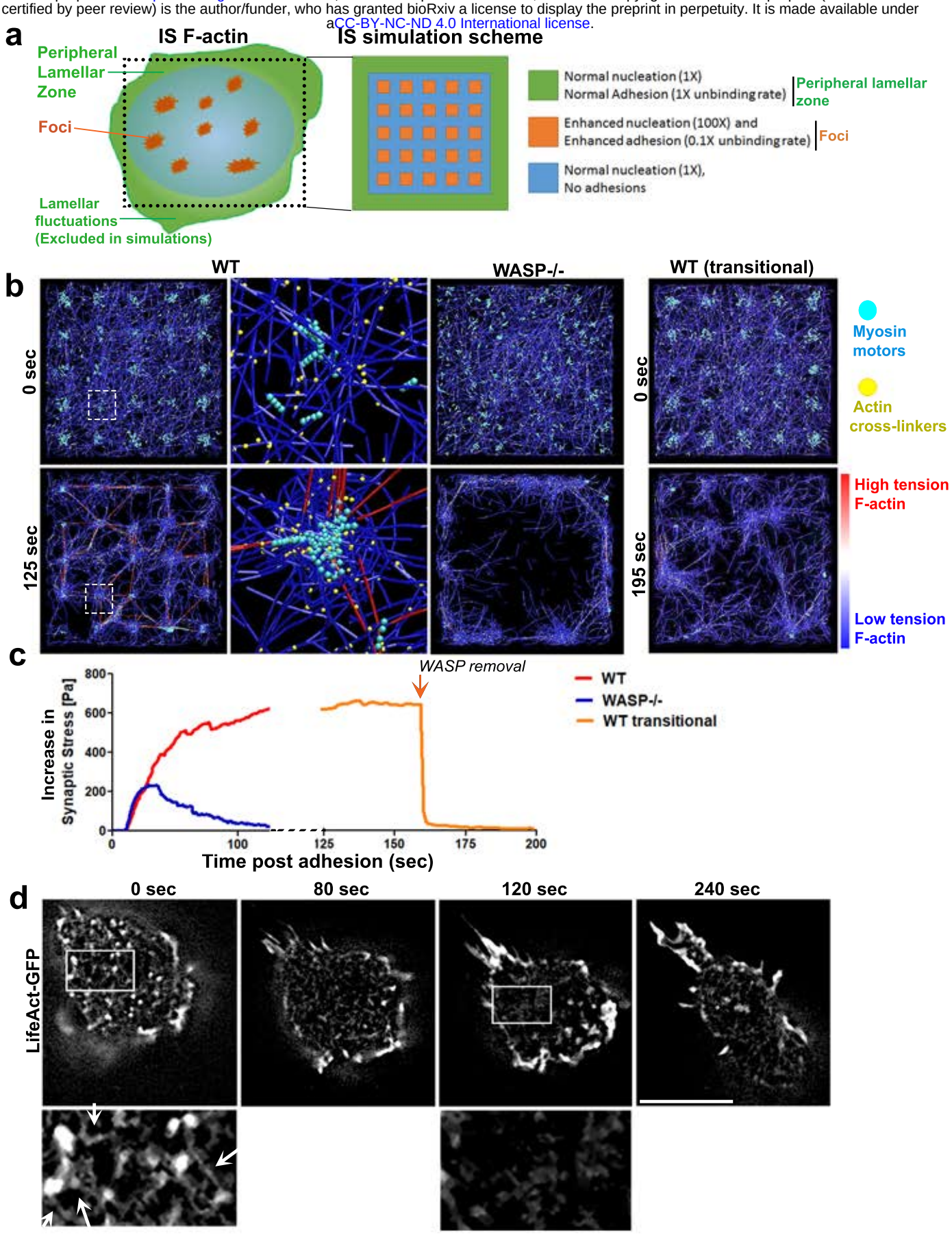

Figure 5

bioRxiv preprint doi: https://doi.org/10.1101/437236; this version posted October 8, 2018. The copyright holder for this preprint (which was not certified by peer review) is the author/funder, who has granted bioRxiv a license to display the preprint in perpetuity. It is made available under aCC-BY-NC-ND 4.0 International license.

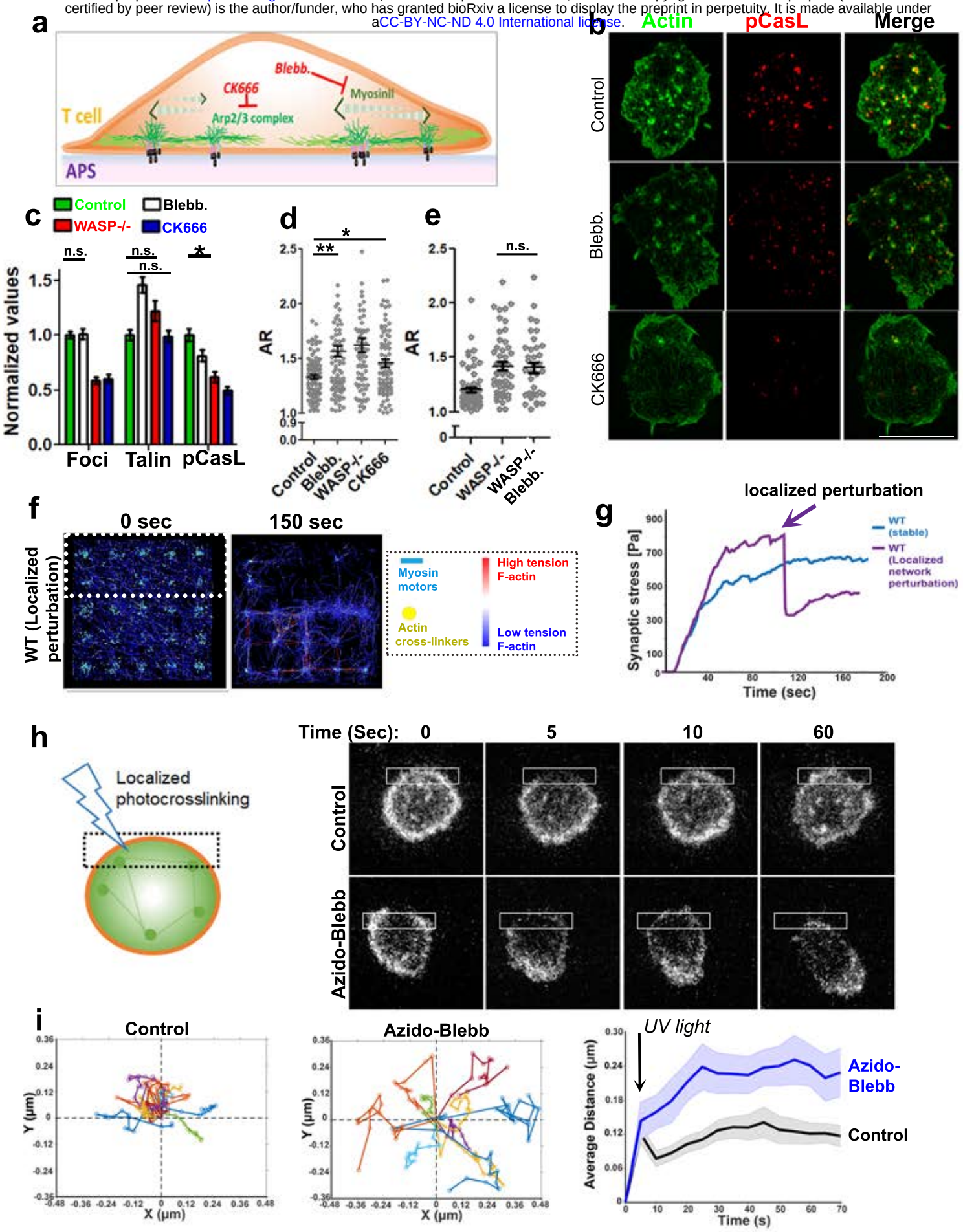

bioRxiv preprint doi: https://doi.org/10.1101/437236; this version posted October 8, 2018. The copyright holder for this preprint (which was not certified by peer review) is the author/funder, who has granted bioRxiv a license to display the preprint in perpetuity. It is made available under aCC-BY-NC-ND 4.0 International license.
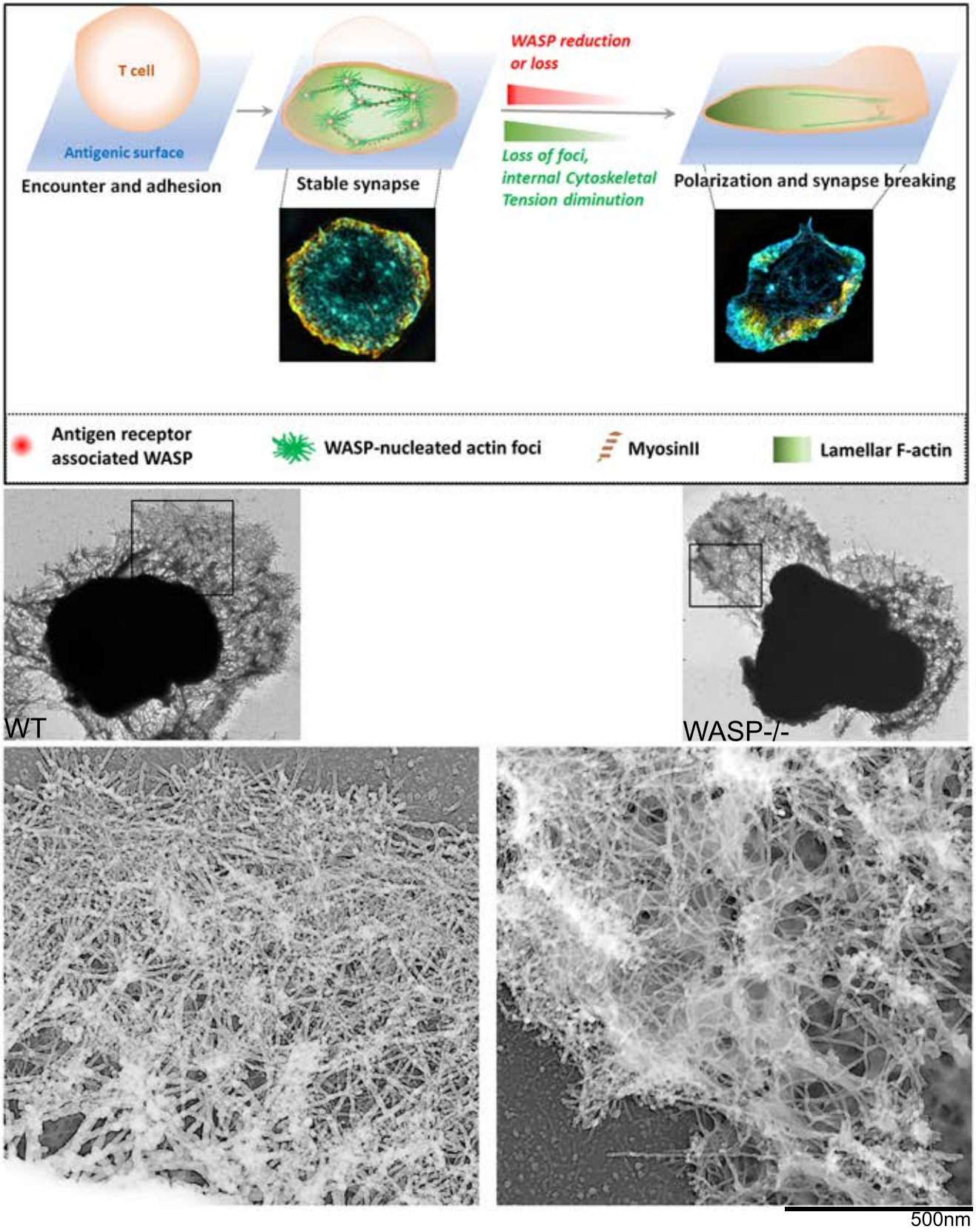
Figure 6